Available online at www.sciencedirect.com
ScienceDirect
Optics Communications 281 (2008) 37–43
OPTICS COMMUNICATIONS
www.elsevier.com/locate/optcom

Optical and holographic properties of Fe+Mn co-doped $Bi_4Ge_3O_{12}$ crystals

Vera Marinova [a,*], Dimitrina Petrova [b], Shiuan Huei Lin [c], Ken Yuh Hsu [d]

[a] Central Laboratory of Optical Storage and Processing of Information, Bulgarian Academy of Science, P.O. Box 95, Sofia 1113, Bulgaria
[b] South West University, Department of Physics, 66 "Ivan Mihailov" Street, 2700 Blagoevgrad, Bulgaria
[c] Department of Electrophysics, National Chiao Tung University, 1001 Ta Hsueh Road, 30050 Hsinchu, Taiwan
[d] Institute of Electro-Optical Engineering, National Chiao Tung University, 1001 Ta Hsueh Road, 30050 Hsinchu, Taiwan

Received 21 January 2007; received in revised form 19 July 2007; accepted 4 September 2007

Abstract

The effect of iron and manganese co-doping on the light-induced, dark- and photoconductivity and holographic properties of $Bi_4Ge_3O_{12}$ crystals in comparison with Fe- and Mn-single doping is studied. Fe+Mn co-doped crystals exhibited strong photochromic effect at room temperature, the photochromic effect being fully reversible by thermal annealing. The observed light-induced absorption changes and non-linear dependence of photoconductivity on light intensities indicate deep and shallow photoactive levels contribution to the charge transport mechanism of Fe+Mn co-doped BGO. Holographic gratings are successfully recorded at different wavelengths and a possibility to extend the photorefractive sensitivity into the red spectral range is demonstrated. It is found furthermore that Fe+Mn-doping combination leads to faster response time during holographic recording, especially after a preliminary exposure with ultraviolet light, in comparison with Fe- and Mn-single doping.

1. Introduction

Recently, a lot of research has been done on photorefractive crystals optimization for holographic data storage and processing of information applications by introducing intrinsic (nonstoichiometric), thermo-chemical (after oxidation/reduction treatments) or extrinsic (doping ions) defects [1,2]. The presence of defects in the crystal structure leads to generation of a charge transfer processes responsible for the photochromic and photorefractive effects – phenomena, which incorporated together, are able to facilitate more efficient and stable holographic recording. The evidence of this approach is recently proposed two-centre recording, which has been realized in Fe+Mn doubly-doped $LiNbO_3$ crystal and persistent (non-volatile) holographic storage has been achieved [3]. Consequently, considerable research efforts have been devoted to doped photorefractive crystals performance and several other appropriate dopant combinations such as Cu, Ce and In, Fe have been proposed [4,5]. Up to now, Fe+Mn doubly doping is the most suitable and effective combination in $LiNbO_3$, which improves both the photosensitivity (strongly enhanced after ultraviolet irradiation) and the diffraction efficiency [6].

Non-doped bismuth germanate $Bi_4Ge_3O_{12}$ (BGO) is one of the few crystals, in which holographic gratings are possible to be recorded at room temperature using ultraviolet range wavelengths [7]. BGO crystals belong to 43*m* point group symmetry (known also as eulytine structure) with four molecules per unit cell. Despite of the storage ability, not much attention has been paid to these materials due to the relatively small electro-optic coefficient and limited photosensitivity.

Doping with appropriate elements is an efficient method to improve the photosensitivity and to increase the density of suitable traps, both necessary for refractive index

* Corresponding author. Tel.: +359 2 979 35 36; fax: +359 2 871 91 65.
E-mail address: vmarinova@optics.bas.bg (V. Marinova).

0030-4018/$ - see front matter © 2007 Elsevier B.V. All rights reserved.
doi:10.1016/j.optcom.2007.09.003

modulation at visible spectral range. BGO crystal structure appears suitable host matrix for extrinsic impurities such as transition metals or rare-earth elements [8]. For example, using an appropriate doping approach, holographic gratings were successfully recorded in Cr-doped BGO crystals at 442 nm [9], in Fe-doped and Mn-doped BGO in a blue-green spectral range [10], in Co- and V-doped BGO crystals at 488 nm and 514 nm [11,12]. Recently, a possibility to extend the photorefractive sensitivity into the red spectral range was demonstrated in Ru-doped BGO [13]. However, the effect of 3d transition metal impurities combination as Fe and Mn on the optical and holographic properties is still missing.

In this paper, we have examined the light-induced and holographic properties of Fe+Mn co-doped BGO and compared the results with single Fe- and Mn-doped crystals, grown at the same conditions and chemical purity of the starting materials. In addition, some material properties relevant to the photorefractive effect as dark- and photoconductivity are characterized. This research was partially motivated due to the fact that BGO crystals are easy to be doped and relatively large crystals with good optical quality are readily available. Moreover with the exhibited photochromic and photorefractive effect Fe+Mn co-doped BGO appears interesting subject for further two-wavelength holographic recording study.

2. Experiment

Fe, Mn and Fe+Mn co-doped BGO crystals were grown with an automatic diameter-weight control system, using the Czochralski technique. Stoichiometric Bi_2O_3:GeO_2 powders were mixed in molar proportion 2:3. Iron and manganese were added into the melt during the crystal growth in the form of Fe_2O_3 and MnO_2 oxides. The doping concentrations in the grown crystals, determined by inductively coupled plasma atomic absorption spectrometry are presented in Table 1. Note that the distribution coefficient of iron into the crystal melt was rather lower than the distribution coefficient of manganese.

The grown crystals were oriented and cut into plates with thickness less than 1 mm for optical and for electrical measurements. For holographic experiments parallelepipeds with edges, oriented with respect to the crystallographic [1 1 0], [1 $\bar{1}$ 0] and [0 0 1] directions, which allows maximum diffraction efficiency to be obtained [15], were prepared.

Optical transmittance spectra were measured on double polished plates in the wavelength range 250–800 nm using Cary 5E model spectrophotometer. Reflectance spectra were done on plates with one polished and one grinded side, using a Perkin Elmer 330 spectrophotometer with etalon references for calibration at 488; 514.5; 576; 632 and 672 nm. The absorption coefficient α (cm^{-1}) was calculated by taking into account the transmittance T and reflection R coefficient and the crystal thickness d:

$$\alpha = -\frac{1}{d}\left(\frac{\sqrt{(1-R)^4 + 4R^2T^2} - (1-R)^2}{2R^2T}\right) \quad (1)$$

All optical measurements were performed at two different states obtained: (i) after thermal annealing and (ii) after 1 h exposure with UV lamp. The thermal annealing (bleaching) process takes place in oxygen atmosphere at 400 °C for 3 h. A 300 W Xe lamp was used for UV light exposure.

Silver surface electrodes with capacitor cell geometry were made on the crystal plates for dark- and photoconductivity characterization. The dark conductivity measurements were carried out using Keithley 6487 Pico-Ammeter/Voltage Supply. A custom made holder with cartridge heaters was used for temperature measurements. The crystal temperature was measured by a Pt thermocouple, mounted just above the sample. The temperature has been controlled with an error of ±1 K. An argon laser source operating at 514 nm was used for photocurrent dependence on the light intensity study. During the photoconductivity measurements we waited several minutes after any change of intensity before the measurement value is taken in order the sample to reach an equilibrium state.

Holographic gratings were recorded in transmission geometry at different wavelengths (Ar^+ laser emitting at 514 nm, He–Ne laser for 633 nm and krypton mixed gas ion laser for 647 nm, respectively) using two-beam interference set-ups. The angle θ between the two interfering beams was 15° and the grating space vector K was parallel to the [0 0 1] direction. During the writing process one of the recording beams (the signal beam) was blocked for about 0.1 s in every 5 s and the reference beam was used to monitor the grating build-up. During the erasure, only the reference beam was incident on the crystal, the signal beam being completely blocked with a shutter. The diffraction efficiency η was defined as the ratio between the diffracted beam intensity and input beam intensity by taking into account the surface reflection. No external electric field was applied.

After each experiment the samples were thermally annealed at 400 °C in order to erase all possible defect traps created during the previous exposure.

Table 1
Doping concentration, dark conductivity (σ_d) and activation energy (E_a) values of Fe+Mn, Fe- and Mn-doped BGO crystals

Sample	Concentr. (cm^{-3})	σ_d $(\Omega\,cm)^{-1}$	E_a (eV)
BGO:Fe+Mn	Fe – 7×10^{18} Mn – 1×10^{18}	9×10^{-14}	0.38 ± 0.04
BGO:Fe	3×10^{18}	5.8×10^{-13}	0.32 ± 0.03
BGO:Mn	5×10^{18}	7.9×10^{-14}	0.4 ± 0.04

3. Results and discussion

3.1. Photochromic effect

Fig. 1a–c shows the absorption spectra of all doped samples. Fe+Mn-doped BGO crystals at their as grown

(initial) state are slightly yellow colored similar to Fe-doped, whereas Mn-doped is green colored. As it seen from Fig. 1a the absorption edge of Fe+Mn co-doped BGO is shifted to the visible spectral range in comparison with non-doped BGO, which absorption spectra is also presented for reference. An absorption peak with a maximum around 500 nm is observed in case of Mn-doped BGO (Fig. 1c). Similar peak, with rather low intensity however is detected for Fe+Mn doubly-doped BGO. No specific peaks were observed for Fe-doped sample (Fig. 1b).

The effect of thermal annealing and UV exposure on optical absorption spectra is also presented in Fig. 1. As can be seen after UV light irradiation a broad absorption band that covers visible spectral region from 800 nm up to the absorption edge was introduced. The photochromic effect observed in Fe+Mn co-doped BGO is similar to those for Fe-doped, which confirms that contribution of iron is larger than that of manganese in our co-doped sample. The photochromic magnitude was stronger in case of Mn-doping (see Fig. 1c). The existence of photochromic behavior has been previously detected in BGO crystals single doped with Fe- and Mn- (however at lower dopants concentration) [14] as well as of Cr- and Co-doped [9,11]. The results presented in Fig. 1b and c are similar to those reported by Zaldo et al. [10] who proposed that UV light irradiation dissociated the native defects in the BGO crystal structure and the created electrons are trapped by transition metal impurities, changing their valence state. In oxide materials like BGO crystals, the photochromic phenomenon is associated mainly with the presence of dopants since the non-doped BGO does not exhibit any appreciable photochromic effect.

It is well known that BGO possess a complex crystal structure, where each Bi^{3+} ion is coordinated by six oxygen ions arranged in a strongly distorted octahedron $[Bi_3O_4]^+$ and each Ge^{4+} ion is surrounded by four oxygen ions arranged in a tetrahedron $[GeO_4]^{4-}$ [16]. Such a structure allows a number of charge trapping sites where the metal impurities are expected to enter in cationic sites: the octahedral Bi^{3+} and/or the tetrahedral Ge^{4+} site. EPR technique has been used to determine the location of Fe and Mn as well as their charge state in BGO host matrix: manganese has been detected in the Bi site as Mn^{2+} [17], whereas Fe^{3+} ions has been detected to substitute in the tetrahedral

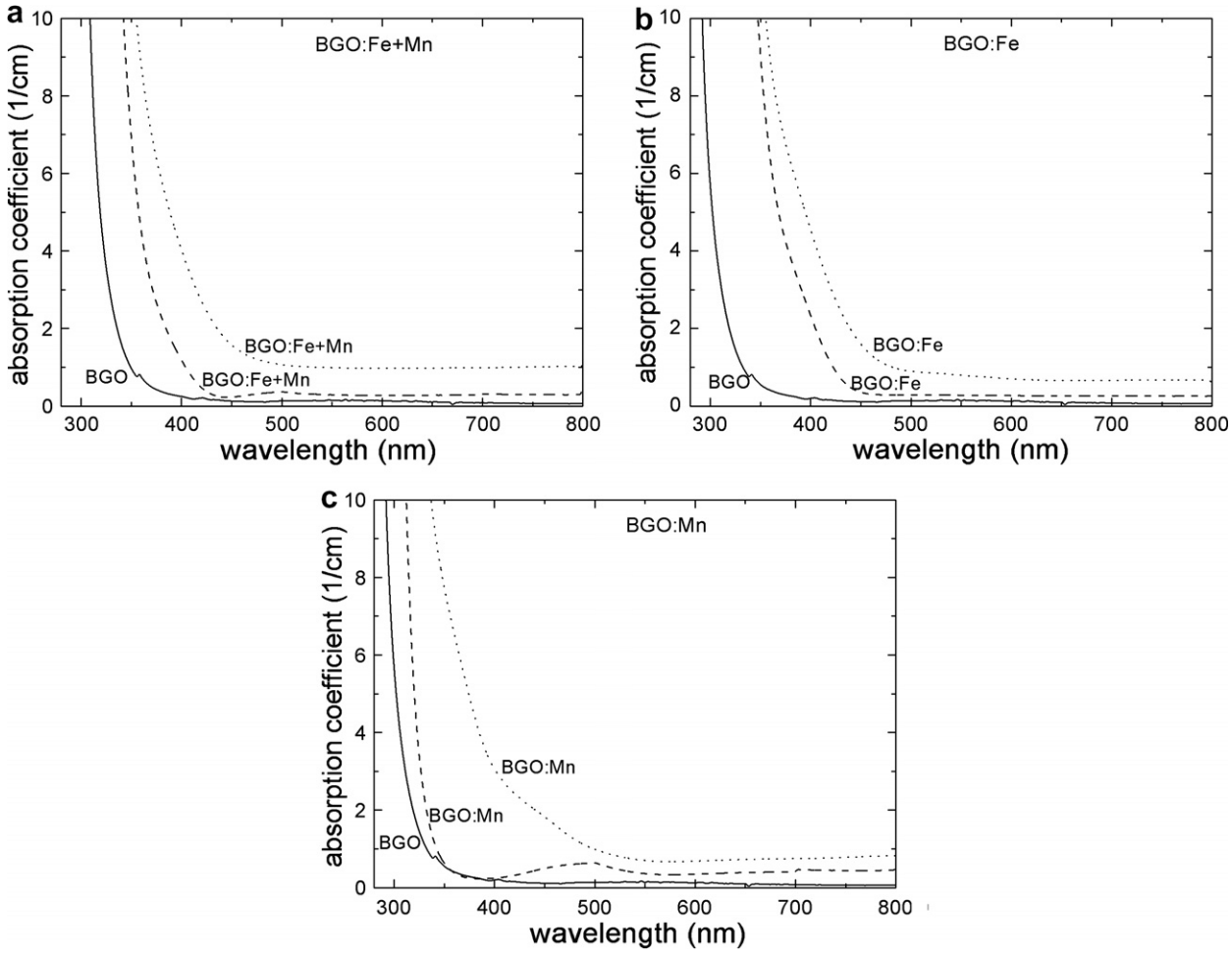

Fig. 1. Absorption coefficient dependence on wavelengths after thermal annealing (dash line) and after UV exposure (dot line) of (a) Fe-doped BGO, (b) Mn-doped BGO and (c) Fe+Mn co-doped BGO. The spectrum (straight line) of non-doped BGO is also presented for reference.

Ge^{4+} site position [18]. The photochromic effect, presented in Fig. 1, is probably due to the valence change of doping elements (Fe^{2+}/Fe^{3+} or Mn^{2+}/Mn^{3+}), caused by the photo-induced charge transfer from the UV sensitive absorption centres via the conduction (valence) band.

Furthermore, the observed photochromism is fully reversible, i.e., the light-induced absorption is possible to be bleached (restored) by subsequent thermal annealing or illumination with visible light. UV exposure treatments have been used to modify the defect structure in a crystal lattice and the corresponding absorption bands during further holographic testing.

3.2. Ohmic characteristics

The dark current j_d dependencies on applied voltage U (V) at room temperature are shown in Fig. 2. The current–voltage characteristics measured in dark conditions show a linear increase for all samples. In addition, a preliminary exposure with UV light leads to lower dark current, which is very important for further holographic recording applications. The calculated values of dark conductivity $\sigma_d = j_d \cdot l/U \cdot A$ (where l is the distance between electrodes and A is the area of electrodes) of preliminary UV illuminated crystals are summarized in Table 1. Mn-doped BGO possess lowest dark conductivity in comparison with other investigated samples. The conductivity values obtained for Fe+Mn and Mn-doped crystals are at the same order of magnitude as previously reported of 5.2×10^{-14} $(\Omega\,\mathrm{cm})^{-1}$ for non-doped BGO [7]. The Fe-doped BGO shows higher dark conductivity, which is evident also from the holographic results.

The dark conductivity temperature dependence is shown in Fig. 3. As can be expected, the conductivity increases with the temperature. The activation energy values were derived from Fig. 3 plots, which follow the Arrhenius law:

$$\sigma = \sigma_0 \exp(-E_a/k_B T) \quad (2)$$

where σ_0 is a pre-exponential factor, E_a is an activation energy for conduction, T is the absolute temperature, k_B is Boltzmann's constant. The data calculated for activation energies are summarized in Table 1. The activation energy value for non-doped BGO crystal, reported by Montemezzani et al. [7] is $E_a = 0.9$ eV. Obviously, Fe and Mn dopants create new centres in BGO inter-band structure, which are probably located above the intrinsic thermal activation level of non-doped BGO. However, these centres probably are located close to each other and in the temperature interval studied the individual contribution is complicated to be precisely separated.

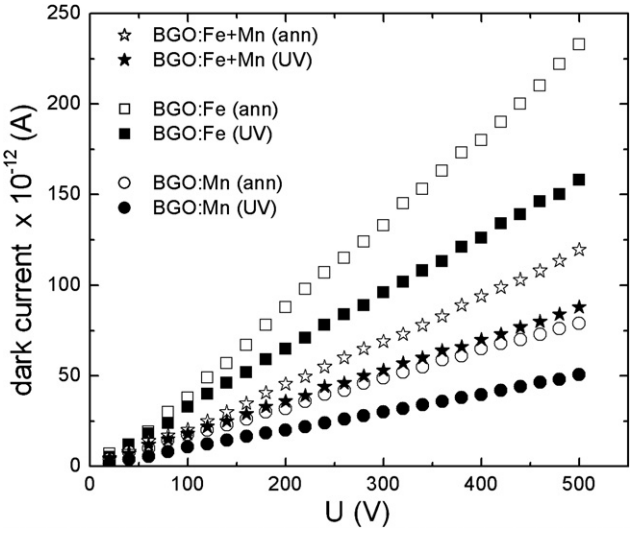

Fig. 2. Volt–ampere characteristics under dark condition at room temperature. Open symbols represents data for samples, measured after thermal annealing, full symbols for samples after UV exposure.

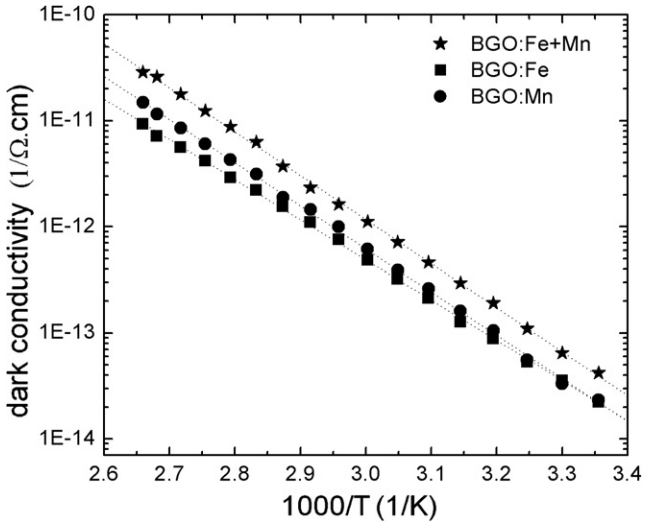

Fig. 3. Arrhenius plot of the dark conductivity σ_d. The symbols are measured data, the dot line is linear fit yielding the activation energy E_a.

The photocurrent dependence on different light intensities of 514 nm and 633 nm wavelengths was measured in an external electric field E_0 (V/cm). The photocurrent was detected by measuring the dark current j_d and the current under light illumination j_i. Subtracting j_d from j_i yields the photocurrent j_{ph} ($j_{ph} = j_i - j_d$). From the photocurrent density the photoconductivity $\sigma_{ph} = j_{ph}/E_0$ was calculated. Fig. 4 shows the photoconductivity σ_{ph} dependence on the light intensity at 514 nm on samples preliminary exposed to UV radiation. As can be seen the laser illumination caused a large increase of conductivity. The photoconductivity determines the speed of the build-up and decay of refractive index change during holographic recording and depends on the ratio of filled to empty traps. It is supposed that decreasing of the number of recombination centres and as a result increasing photo-carriers lifetime leads to the photoconductivity increase. The photoconductivity increases nonlinearly with the light intensity in case of Fe+Mn co-doping as well as of Fe-doped crystal. However, a saturation effect is observed of Mn-doped BGO.

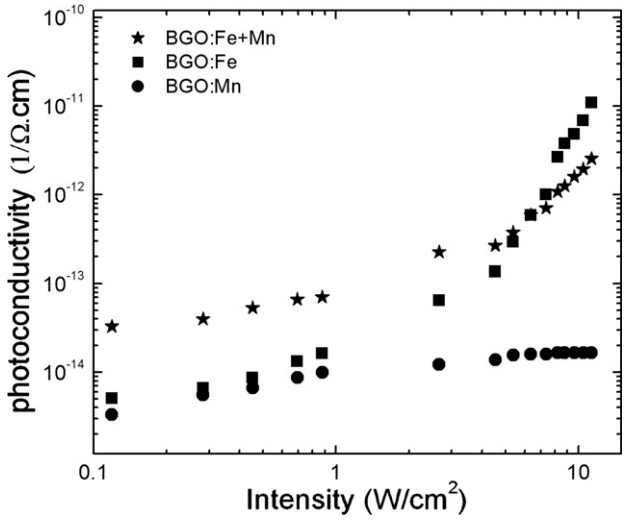

Fig. 4. Photoconductivity σ_{ph} dependence on the light intensity at wavelength of 514 nm.

Similar behavior though with lower photoconductivity values for all samples has been detected using 633 nm light beam.

The light-induced absorption changes and non-linear dependence of photoconductivity on light intensities indicate that deep and shallow photoactive levels contribute together to the charge transport mechanism of Fe- and Fe+Mn-doped BGO.

3.3. Holographic behavior

In this paragraph we present the temporal evolution of writing and erasing of holographic gratings in samples preliminary irradiated with UV light. Fig. 5a–c compares the recording and erasing characteristics measured at different wavelengths, using similar writing geometry and beam intensities. Moreover, the holographic behavior of thermally annealed samples at selected wavelength is presented as additional plot of Fig. 5b.

As can be seen in Fig. 5a after the fast initial response and a maximum of the diffraction efficiency, a decay (continuous decreasing) of diffracted signal beam intensity during recording process has been detected for Fe-doped at 514 nm. Two maximums and steady-state behavior during the holographic recording temporal evolution in preliminary UV exposed samples has been reported by Zaldo et al. [10] for Fe-doped BGO at 457 nm and 514 nm and for co-doped BGO at 488 nm [11]. A transient behavior of the diffraction efficiency has been observed in $Bi_{12}SiO_{20}$ and $KNbO_3$ crystals however [20,21]. The origin of such response has been assigned to the simultaneous diffusion of electrons and holes creating secondary space charge grating, which reduces the space charge electric field. At longer recording wavelengths (see Fig. 5b,c), Fe-doped BGO shows a typical single exponential behavior [15] with response time of 12 min at 633 nm and 16 min for 647 nm, respectively. The Fe-doped possess faster response time than Mn-doped BGO, as well as shows faster decay time constants during the erasure process in comparison with other samples.

The writing dynamics behavior observed in Mn-doped BGO follows single exponential dependence for all investigated wavelengths. In addition, Mn-doped is the slowest one sample regarding to the response time. No complex dynamic such in case of Fe- and Fe+Mn co-doped was observed for Mn-doped BGO, even the recording time was prolonged. The detected holographic behavior together with the light intensity dependence of photocurrent support the assumption, that only one kind of charge carrier dominates during the charge transport of Mn-doped BGO [19].

Fe+Mn co-doped BGO, however, shows more complex holographic behavior, starting with fast growth during the first few minutes (depending on the recording wavelength), followed by the diffracted signal decreasing and finally the signal increased, approaching to the steady-state value after prolonged time of recording. The decay time constant is also extended to longer time (confirmed by dark current measurements), suggesting that Fe+Mn combination could be useful for two wavelengths recording.

The complex behavior of diffraction efficiency in Fe+Mn co-doped BGO is possible to be assumed as a result of two phenomena: (i) photorefractive response with transient character arising from the redistribution of electron and holes, which finally reduces the space charge electric field by creating secondary space charge grating and (ii) the photochromic grating, arising almost simultaneously with the photorefractive one. In order to estimate the real contribution of the photochromic grating to the total diffraction efficiency, more detailed study of the evolution of optical absorption coefficient under the same experimental conditions as used to write the holograms are necessary.

One can assume that Fe addition shows dominant contribution in Fe+Mn co-doped BGO samples as it plays major role in the photochromic properties as it was reported in previous paragraph.

Furthermore, it was found that the holographic recording dynamics strongly depends on the preliminary history of the samples. The diffracted light is very low when the crystals are in a bleached state. An example is shown as attached plot of Fig. 5b for 633 nm (dashed lines) and the samples show very similar behavior for shorter recording wavelengths as well. However, after UV irradiation, the diffraction efficiency increases more than ten times in case of Fe+Mn-doped BGO for example. On the same time, even at annealed state the grating kinetics possess similar complex behavior as in the case after UV exposure, which suggested that the photorefractive contribution probably is a dominant effect during the holographic recording. Much weaker contribution of the photochromic effect than the refractive index modulation has been reported of Cr-doped BGO also [9].

In our assumption, Fe ions probably occupied traps, located most shallow to the conduction (valence) band in

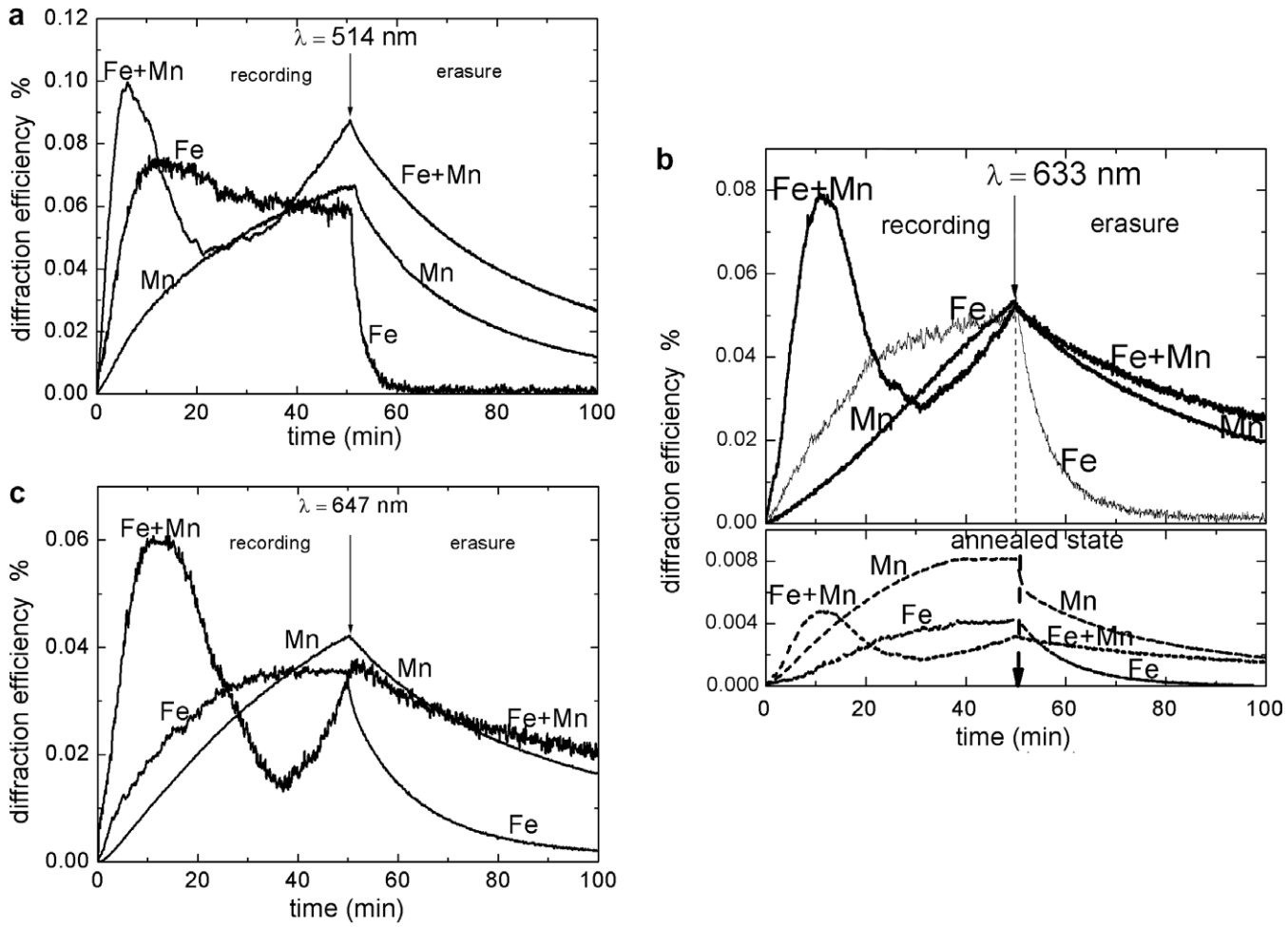

Fig. 5. Holographic recording-erasure cycles and experimental conditions at: (a) $\lambda = 514$ nm, grating spacing $\Lambda = 0.45$ μm, recording intensity 15 mW/cm^2; (b) $\lambda = 633$ nm, grating spacing $\Lambda = 0.61$ μm, recording intensity 15 mW/cm^2; attach plot-samples after thermal annealing (dash line) (c) $\lambda = 647$ nm; grating spacing $\Lambda = 0.64$ μm, recording intensity 10 mW/cm^2.

respect to the position of the deep traps created by Mn. This could be confirmed with the measured non-linear dependence on photoconductivity on the illuminating light intensity (see Fig. 4). In addition, other defects, different from Fe and Mn impurities could contribute to the observed process, like intrinsic defects of BGO crystal. In that case, it could be supposed that Fe and Mn ions act as traps, whereas the donors are intrinsic defects of non-doped BGO.

4. Conclusion

It is shown that by Fe+Mn-doping combination the absorption edge of BGO crystals was shifted to the visible wavelengths and crystals exhibited a reversible photochromic effect at room temperature, which could be bleached by thermal annealing.

Fe+Mn co-doping increase the response time and diffraction efficiency during holographic recording in comparison with Fe- and Mn-single doping. Furthermore, it was found that the writing kinetics of the recorded holograms depends on the preliminary illumination with UV light. Co-doped samples show complex holographic behavior, characterized with fast initial growth, followed by diffraction efficiency decrease and finally increasing again. Such dynamics suggesting contribution of two processes involved simultaneously: photorefractive response with transient character arising from the redistribution of electron and holes with competitive behavior and photochromic grating evolving almost simultaneously with the photorefractive one.

Fe-addition shows dominant effect in both the photochromic behavior and holographic properties of Fe+Mn co-doped BGO samples.

Using the ability of Fe+Mn co-doped BGO to achieve higher diffraction efficiency and faster response time, we hope that, with further suitable selection of doping concentrations, it would be possible to optimize the photorefractive performance at visible and near infrared wavelengths range.

Acknowledgements

Financial support by the National Science Fund F-1405, Bulgaria and by Taiwan–Bulgarian collaboration program agreement Contract # NSC 95-2911-I-009-005 is gratefully

acknowledged. Doped BGO crystals were grown in the Crystal Growth Laboratory, Institute of Solid State Physics, Bulgarian Academy of Science.

References

[1] H.J. Coufal, D. Psaltis, G.T. Sincerbox (Eds.), Holographic Data Storage, Springer-Verlag, Berlin Heidelberg, 2000.
[2] K. Buse, Appl. Phys. B 64 (1997) 391.
[3] K. Buse, A. Adibi, D. Psaltis, Nature 393 (1998) 665.
[4] Y. Liu, L. Liu, C. Zhou, L. Xu, Opt. Lett. 25 (2000) 908.
[5] G. Zhang, Y. Tomita, X. Zhang, J. Xu, Appl. Phys. Lett. 81 (2002) 1393.
[6] A. Adibi, K. Buse, D. Psaltis, J. Opt. Soc. Am. B 18 (2001) 584.
[7] G. Montemezzani, St. Pfandler, P. Gunter, J. Opt. Soc. Am. B 9 (1992) 1110.
[8] P.A. Williams, A.H. Rose, K.S. Lee, D.C. Conrad, G.W. Day, P.D. Hale, Appl. Opt. 35 (1996) 3562.
[9] E. Moya, L. Contreras, C. Zaldo, J. Opt. Soc. Am. B 5 (1988) 1737.
[10] C. Zaldo, E. Moya, F. Magana, L. Kovacs, K. Polgar, J. Appl. Phys. 73 (1993) 2114.
[11] C. Zaldo, E. Dieguez, Opt. Mater. 1 (1992) 171.
[12] V. Marinova, Shiuan Huei Lin, Mei-Li Hsieh, M.M. Gospodinov, Ken Yuh Hsu, Opt. Mem. Neural Network 11 (2002) 211.
[13] V. Marinova, S.H. Lin, K.Y. Hsu, J. Appl. Phys. 98 (2005) 113527.
[14] L. Kovacs, E. Moya, K. Polgar, F.J. Lopez, C. Zaldo, Appl. Phys. A 52 (1991) 307.
[15] P. Yeh, Introduction to Photorefractive Nonlinear Optics, Wiley Interscience, New York, 1993.
[16] A.A. Kaminskii, D. Schultze, B. Hermoneit, S.E. Sarkisov, L. Li, J. Bohm, P. Reiche, R. Ehlert, A.A. Mayer, V.A. Lomonov, V.A. Balashov, Phys. Stat. Sol. (a) 33 (1976) 737.
[17] D. Bravo, L. Arizmendi, M. Aguilar, F.J. Lopez, J. Phys. Condens. Mat. 2 (1990) 10123.
[18] A. Martin, D. Bravo, E. Dieguez, F.J. Lopez, Phys. Rev. B 54 (1996) 12915.
[19] K. Buse, Appl. Phys. B 64 (1997) 273.
[20] F.P. Strohkendl, J. Appl. Phys. 65 (1989) 3773.
[21] G. Montemezzani, Photorefractive gratings: fixing and recording in the visible and ultraviolet, PhD thesis, Zurich, 1993.